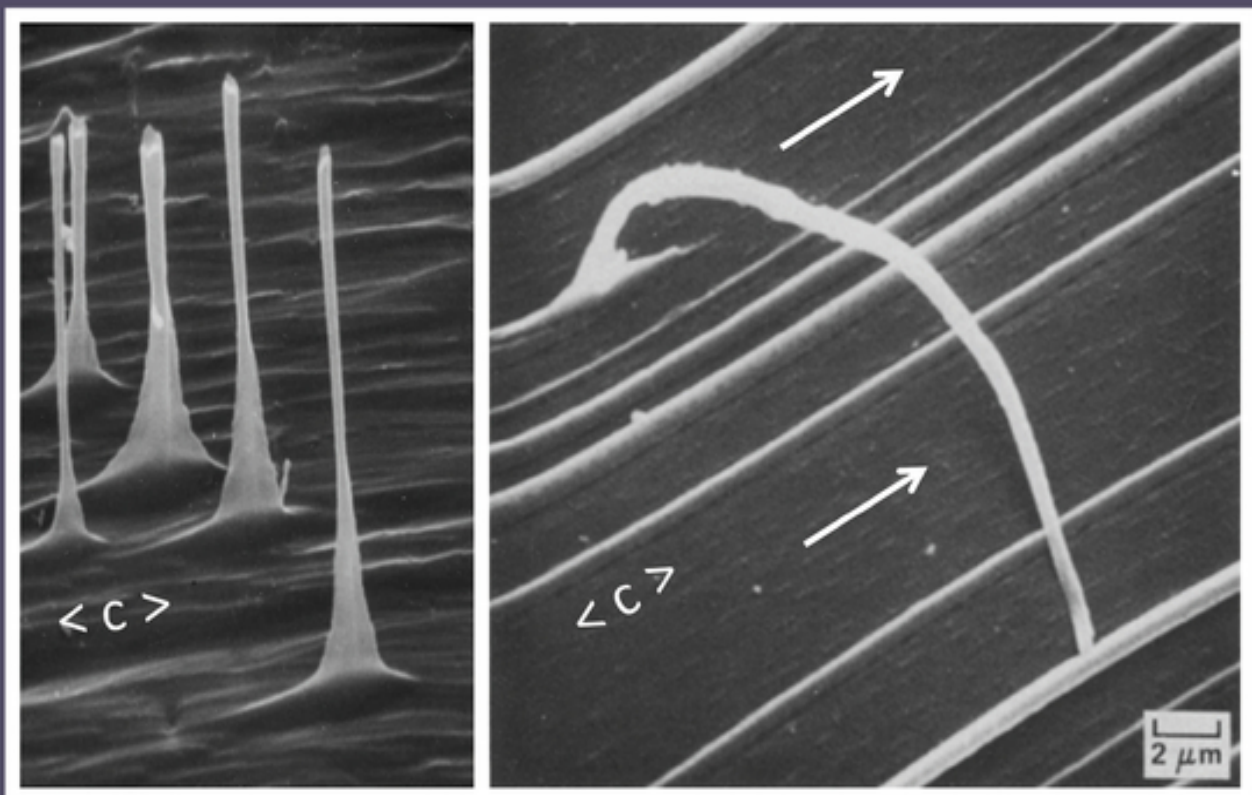


ENGINEERING PHYSICS OF HIGH-TEMPERATURE MATERIALS

METALS, ICE, ROCKS, AND CERAMICS



NIRMAL K. SINHA ■ SHOMA SINHA

WILEY

Table of Contents

[Cover](#)

[Title Page](#)

[Metals, Ice, Rocks, and Ceramics](#)

[Copyright Page](#)

[Dedication](#)

[Acknowledgments](#)

[Engineering Physics of High-Temperature Materials](#)

[Preface](#)

[1 Importance of a Unified Model of High-Temperature Material Behavior](#)

[1.1 The World's Kitchens - The Innovation Centers for Materials Development](#)

[1.2 Trinities of Earth's Structure and Cryosphere](#)

[1.3 Earth's Natural Materials \(Rocks and Ice\)](#)

[1.4 Rationalization of Temperature: Low and High](#)

[1.5 Deglaciation and Earth's Response](#)

[1.6 High-Temperature Deformation: Time Dependency](#)

[1.7 Strength of Materials](#)

[1.8 Paradigm Shifts](#)

[References](#)

[2 Nature of Crystalline Substances for Engineering Applications](#)

[2.1 Basic Materials Classification](#)

[2.2 Solid-state Materials](#)

[2.3 General Physical Principles](#)

[2.4 Glass and Glassy Phase](#)

[2.5 Rocks: The Most Abundant Natural Polycrystalline Material](#)

[2.6 Ice: The Second Most Abundant Natural Polycrystalline Material](#)

[2.7 Ceramics](#)

[2.8 Metals and Alloys](#)

[2.9 Classification of Solids Based on Mechanical Response at High Temperatures](#)

[References](#)

[3 Forensic Physical Materialogy](#)

[3.1 Introduction](#)

[3.2 Polycrystalline Solids and Crystal Defects](#)

[3.3 Structure and Texture of Natural Hexagonal Ice, \$I_h\$](#)

[3.4 Section Preparation for Microstructural Analysis](#)

[3.5 Etching of Prepared Section Surfaces](#)

[3.6 Sublimation Etch Pits in Ice, \$I_h\$](#)

[3.7 Etch-Pitting Technique for Dislocations](#)

[3.8 Chemical Etching and Replicating of Ice Surfaces](#)

[3.9 Displaying Dislocation Climb by Etching](#)

[3.10 Thermal Etching: An Unexploited Materialogy Tool](#)

[References](#)

[4 Test Techniques and Test Systems](#)

[4.1 On the Strength of Materials and Test Techniques](#)

[4.2 Static Modulus and Dynamic Elastic Modulus](#)

[4.3 Thermal Expansion Over a Wide Range of Temperature](#)

[4.4 Creep and Fracture Strength](#)

[4.5 Bending Tests](#)

[4.6 Compression Tests - Uniaxial, Biaxial, and Triaxial](#)

[4.7 Tensile and/or Compression Test System](#)

[4.8 Stress Relaxation Tests \(SRTs\)](#)

[4.9 Cyclic Fatigue](#)

[4.10 Acoustic Emission \(AE\) and/or Microseismic Activity \(MA\)](#)

[4.11 Tempering of Structural and Automotive Glasses](#)

[4.12 Specimen Size and Geometry: Depending on Material Grain Structure](#)

[4.13 In Situ Borehole Tests: Inspirations from Rock Mechanics](#)

[References](#)

[5 Creep Fundamentals](#)

[5.1 Overview](#)

[5.2 On Rheology and Rheological Terminology](#)

[5.3 Forms of Creep and Deformation Maps](#)

[5.4 Grain-Boundary Shearing or Sliding](#)

[5.5 Creep Curves - Classical Primary, Secondary, and Tertiary Descriptions](#)

[5.6 Phenomenology of Primary Creep in Metals, Ceramics, and Rocks](#)

[5.7 Primary Creep in Ice: Launching SRRT Technique and EDEV Model](#)

[5.8 Grain-Boundary Shearing \(gbs\) and Grain-Size Dependent Delayed Elasticity](#)

[5.9 Generalization of EDEV Model: Introduction of Grain-Size Effect](#)

[5.10 Logarithmic Primary Creep: An Alternative Form of the EDEV Model](#)

[5.11 Shifting Paradigms: Emphasizing Primary Creep of Polycrystalline Materials](#)

[5.12 SRRT for Primary Creep and EDEV Model of a Titanium-Base Superalloy \(Ti-6246\)](#)

[5.13 SRRT for Primary Creep and EDEV Model for a Nickel-Base Superalloy \(Waspaloy\)](#)

[5.14 SRRT for Primary Creep of a Nickel-Rich Iron-Base Alloy \(Discaloy\)](#)

[5.15 SRRTs for Primary Creep and EDEV Model of a Nickel-Base Superalloy \(IN-738LC\)](#)

[5.16 EDEV-Based Strain-Rate Sensitivity of High-Temperature Yield Strength](#)

[5.17 Single-Crystal \(SX\) Superalloy Delayed Elasticity and \$\gamma/\gamma'\$ Interface Shearing](#)

[5.18 Creep, Steady-State Tertiary Stage, and Elasto-Viscous \(EV\) Model for Single Crystals](#)

[5.19 Creep Fracture and EV Model for CMSX-10 SXs](#)

[5.20 Fracture and Inhomogeneous Deformation](#)

[5.21 Dynamic Steady-State Tertiary Creep of Several Nickel-Base SXs](#)

[References](#)

[6 Phenomenological Creep Failure Models](#)

[6.1 Creep and Creep Failure](#)

[6.2 Steady-State Creep](#)

[6.3 Commonly Used Creep Experiments and Strength Tests](#)

[6.4 Modeling Very Long-Term Creep Rupture from Short-Term Tests](#)

[6.5 High-Temperature Low-Cycle Fatigue \(HT-LCF\) and Dwell Fatigue](#)

[6.6 Crucial Tests on Rate Sensitivity of High-Temperature Strength](#)

[6.7 Rational Approach Inspired by the Principle of "Hindsight 20/20"](#)

[References](#)

[7 High-Temperature Grain-Boundary Embrittlement and Creep](#)

[7.1 Fracture and Material Failure](#)

[7.2 Grain Size Effects on Strength](#)

[7.3 Grain-Boundary Shearing \(gbs\) Induced Crack Initiation](#)

[References](#)

[8 Microstructure and Crack-Enhanced Elasto - Delayed-Elastic - Viscous Models](#)

[8.1 Physics-Based Holistic Model Approach](#)

[8.2 Kinetics of Microcracking and Structural Damage](#)

[8.3 Microcrack-Enhanced EDEV Model](#)

[8.4 EDEV-Based Algorithm for Constant Strain Rate, Encompassing Cracking](#)

[8.5 Constant Stress, Crack-Enhanced Creep: EDEV Predictions](#)

[8.6 Cyclic Fatigue](#)

[8.7 Crack Healing or Closure of w-Type Voids Generating r-Type Cavities](#)

References

9 Stress Relaxation at High Temperatures

9.1 The Role of Stress Relaxation Tests at High Temperatures

9.2 Constitutive Equations without Effect of Grain Size

9.3 Temperature and Grain-Size Effects on SR

9.4 Forecasting Grain-Size Effects on SR in Pure Ice Based on EDEV Equation

9.5 High-Temperature Forming, Delayed Spring-Back, and Grain-Size Effects on SR in Metals

References

10 Ice Age and Intraglacial Depression and Postglacial Rebound of Earth's Crust

10.1 Tectonic Plates, Lake Ice, and High-Temperature Materials: What Is the Connection?

10.2 On Glaciers and Oceanic Ice Cover: Past and Present

10.3 Dow's Lake Studies

10.4 Elasto-Delayed-Elastic (EDE) Theory for Plates

References

11 Plate Tectonics and Polar Sea Ice

11.1 Retrospective Introduction

11.2 Earth and Plate Tectonics

11.3 Scale of Observations

11.4 Vertical Temperature Profiles of Earth and Ice Sheet

11.5 Time-Temperature Shift Function

11.6 Nonlinear, Grain-Size-Dependent Delayed Elasticity (Anelasticity) of Mantle

[11.7 Stress Field of Earth's Crust](#)

[11.8 Koyna and Warna Dams in India and Reservoir-Triggered Seismicity \(RTS\)](#)

[11.9 Movement of Tectonic Plates, Indentation, and Fracture](#)

[11.10 Looking Forward](#)

[References](#)

[Index](#)

[End User License Agreement](#)

List of Tables

Chapter 2

[Table 2.1 Comparison of the properties of some basic carbon allotropes.](#)

[Table 2.2 Nominal chemical compositions \(wt. %\) of Nimonic 90 \(Betteridge a...](#)

Chapter 5

[Table 5.1 Material parameters for ice \(S-2 and equiaxed\)\), Ti-6246, Waspalo...](#)

Chapter 7

[Table 7.1 Creep parameters for pure S-2 ice obtained independently from cre...](#)

List of Illustrations

f05

[Figure P.1 Delayed elastic strain \(des\) recovery. \(a\) constant-stress creep ...](#)

[Figure P.2 “Trishul” \(trident\) of the two primary – North \(N\) and South \(S\) ...](#)

Chapter 1

[Figure 1.1 Harappan style of brick production from clay. \(a\) Process of sun ...](#)

[Figure 1.2 Melting points of some pure metals and ice.](#)

[Figure 1.3 Scanning electron micrograph of \(a\) a vertical section of a brine...](#)

[Figure 1.4 Short-term \(200 s\) and longer-term \(2341 s\) tensile SRRTs on a si...](#)

[Figure 1.5 Results of Figure 1.4 shown in a logarithmic timescale, illustrat...](#)

[Figure 1.6 Strain-time curves, showing rise time to apply full load \(<1 s\), ...](#)

[Figure 1.7 Stress-strain diagram. \(a\) Two values of elastic modulus, \$E\$, and ...](#)

[Figure 1.8 Stress dependence of average viscous strain rate during primary c...](#)

Chapter 2

[Figure 2.1 Basic crystal lattice structures: \(a\) BCC, \(b\) FCC, and \(c\) HCP c...](#)

[Figure 2.2 Stacking sequence in \(a\) FCC and \(b\) HCP crystals.](#)

[Figure 2.3 Typical pressure versus temperature of a one-component system. \$T\$](#)

[Figure 2.4 Sample phase diagram schematic for a binary XY system. \(a\) Simple...](#)

[Figure 2.5 Schematic of common point defects in crystals, including a vacanc...](#)

[Figure 2.6 Schematic of the basic motion or propagation of an edge dislocati...](#)

[Figure 2.7 Schematic of the basic motion or propagation of a screw dislocati...](#)

[Figure 2.8 Composition of a typical soda-lime container glass given in weigh...](#)

[Figure 2.9 Thermally tempered lath with \(a\) parabolic stress distribution in...](#)

[Figure 2.10 Temperature dependence of the CLTE for a lapped and polished lat...](#)

[Figure 2.11 Temperature dependence of Young's modulus, \$E\$, for commercially a...](#)

[Figure 2.12 Simplified phase diagram of water showing stable ice polymorphs....](#)

[Figure 2.13 Snowflake and hexagonal ice. \(a\) Natural snowflake photographed ...](#)

[Figure 2.14 Schematic of \(a\) NaCl structure with sixfold polyhedral coordina...](#)

[Figure 2.15 Iron-carbon phase diagram demonstrating the main phases under at...](#)

[Figure 2.16 Schematic of cuboidal \$\gamma'\$ \(\$\text{Ni}_3\(\text{Al,Ti}\)\$ \) precipitates within a \$\gamma\$ \[F...](#)

[Figure 2.17 Dependence of strain age cracking susceptibility based "weldabil...](#)

[Figure 2.18 Chemical composition diagrams of three nickel-base superalloys. ...](#)

[Figure 2.19 Schematic of primary and secondary \$\alpha\$ -phases within a \$\beta\$ -phase mat...](#)

Chapter 3

[Figure 3.1 \(a\) Three-dimensional drawing of an idealized lattice structure s...](#)

[Figure 3.2 Schematic of etch pitting along dislocation core and SEM of repli...](#)

[Figure 3.3 Schematic of etch pitting along dislocation core and SEM of repli...](#)

[Figure 3.4 Nonbasal \(pointing upward\) and basal \(horizontal\) dislocations....](#)

[Figure 3.5 Optical images of triple points in transparent, pure columnar-gra...](#)

[Figure 3.6 SEM images of etched and replicated surfaces of ice. \(a\) Hexagona...](#)

[Figure 3.7 SEM images of etched and replicated surfaces of ice. \(a\) Few basa...](#)

[Figure 3.8 SEM images of etched and replicated surfaces of ice. \(a\) Arrested...](#)

[Figure 3.9 SEM of etch pits with core whiskers in slip bands and multitude o...](#)

[Figure 3.10 Four types of ice structure.](#)

[Figure 3.11 NRCC large-field polariscope for observations of circular thin s...](#)

[Figure 3.12 Images from the large field-of-view NRCC polariscope. \(a\) Concen...](#)

[Figure 3.13 Orientation of ion-exchanged cracks on the surface of a 25 mm wi...](#)

[Figure 3.14 Sublimation pits in ice. Note especially the shape of the pits f...](#)

[Figure 3.15 Optical micrographs of replicated surfaces exhibiting two differ...](#)

[Figure 3.16 SEM showing many shallow etch tracts for rapidly moving traffic ...](#)

[Figure 3.17 Micrographs of ice replicas. \(a\) Optical micrograph exhibiting a...](#)

[Figure 3.18 Sketch of relevant parameters for etching in air/gas environment...](#)

[Figure 3.19 Sketch of a thermal-etching box with transparent glass bottom an...](#)

[Figure 3.20 Optical micrograph showing grain-size distribution in spat-coole...](#)

[Figure 3.21 Optical micrograph of a horizontal thin section \(prepared by DMT...](#)

[Figure 3.22 Optical micrograph of microtomed and thermally etched surface, n...](#)

[Figure 3.23 Thermally etched surface, normal to the long axis of a grain of ...](#)

[Figure 3.24 Optical image of thermally etched biaxially deformed S-3 sea ice...](#)

Chapter 4

[Figure 4.1 Experimentally determined and calculated \(solid lines\) dependence...](#)

[Figure 4.2 Frequency dependence of the effective elastic modulus of cast, HI...](#)

[Figure 4.3 Stress-strain hysteresis loop for SRRT on nickel-base Waspaloy at...](#)

[Figure 4.4 Stress-strain hysteresis loop for SRRT for a creep time of 300 s ...](#)

[Figure 4.5 Temperature dependence of “static” Young's modulus of HIPed and h...](#)

[Figure 4.6 Thermal strain in nickel-base superalloy IN-738LC in the temperat...](#)

[Figure 4.7 Four-point bending arrangements. \(a\) Home-made single-lever loadi...](#)

[Figure 4.8 Interference patterns, produced by a Babinet compensator in monoc...](#)

[Figure 4.9 Stress distributions in bending for nonlinear viscoelastic materi...](#)

[Figure 4.10 Specimen with five spot-welded thermocouples in a three-zone fur...](#)

[Figure 4.11 Front and rear views of SRRT test setup showing a three-zone fur...](#)

[Figure 4.12 SRRT of 724 MPa and 200 s at 732 °C \(1005K\) for Waspaloy forging...](#)

[Figure 4.13 Schematics of the stress relaxation process for an imposed const...](#)

[Figure 4.14 Relaxation of stress \(stress-induced birefringence\) in a glass l...](#)

[Figure 4.15 SRRT result for Waspaloy forgings. \(a\) For 574 MPa, about 80% of...](#)

[Figure 4.16 Densification in snow. \(a\) Microstructure of aircraft-compacted ...](#)

[Figure 4.17 Rectangular specimen \(250 × 100 × 50 mm\) of translucent columnar...](#)

[Figure 4.18 Evolution of through-thickness profile of stress \(birefringence\)...](#)

[Figure 4.19 Thermal tempering in 6.5 mm thick glass plates. \(a\) Evolution of...](#)

[Figure 4.20 NRCC-BHI schematics. \(a\) Overview; \(b\) NRC-BHI inside a 150 mm d...](#)

[Figure 4.21 The senior author with the entire NRCC-BHI test system at "Hobso...](#)

[Figure 4.22 NRCC-BHI tests in S-1 ice. \(a\) Scattered light and \(a'\) polarize...](#)

Chapter 5

[Figure 5.1 Creep of structurally stabilized plate glass at 547.5 °C in four-...](#)

[Figure 5.2 Creep of plate glass for 80, 200, and 400 kg cm⁻² at severa...](#)

[Figure 5.3 Normalized and temperature compensated creep in glass reduced to ...](#)

[Figure 5.4 Application of the shift functions to individual SRT results: \(a\)...](#)

[Figure 5.5 Creep and recovery of Aheim dunite at \(a\) 1473 K and initial stre...](#)

[Figure 5.6 Variation of initial strain with applied stress at 233 K \(0.85 \$T_m\$ \)](#)

[Figure 5.7 Creep and recovery of transversely isotropic \(orthotropic\) S-2 ic...](#)

[Figure 5.8 Primary-creep of S-2 ice for 0.49 MPa \(\$5.2 \times 10^{-5} E\$ \) reduce...](#)

[Figure 5.9 Calculated creep rate versus stress at different creep times appr...](#)

[Figure 5.10 Calculated dependence of \$\bar{x}_t\$ on total strain \$\varepsilon_t\$ for various \$g...\$](#)

[Figure 5.11 Calculated strain dependence of the ratio of delayed elastic \(gb...](#)

[Figure 5.12 Stress dependence of the ratio of delayed \(gbs\) to total strain,...](#)

[Figure 5.13 Grain-size dependence of \$\dot{\epsilon}_t / \dot{\epsilon}_v\$ at loading time of \$10^4\$ s, computed...](#)

[Figure 5.14 SRRTs for one specimen \(A\) of forged Ti-6246 \(Ti-6Al-2Sn-4Zr-6Mo...](#)

[Figure 5.15 Four \$\epsilon_d\$ and \$\epsilon_v\$ data and recorded creep strain \(from \$\epsilon...\$](#)

[Figure 5.16 SRRT curves for one specimen, A, of Ti-6246 at 873 K \(\$0.45 T_m\$ \) f...](#)

[Figure 5.17 Dependence of viscous strain rate and des during primary creep o...](#)

[Figure 5.18 Optical micrograph of Waspaloy forgings.](#)

[Figure 5.19 SRRT of 390 MPa and 350 MPa for Waspaloy at 1005 K \(\$0.62 T_m\$ \). \(a...](#)

[Figure 5.20 SRRT for \$t_{rlx}\$ of 200 s for 724 MPa \(\$4.19 \times 10^{-3} E\$ \) at 1005...](#)

[Figure 5.21 Stress dependence of \$\epsilon_d / \epsilon_v\$ from SRRT on a single speci...](#)

[Figure 5.22 Dependence of des on \$\ln\(t_{rlx} + 1\)\(\sigma/E\)\$. \$s\$, for \$E = 172.66\$ GPa...](#)

[Figure 5.23 Stress dependence of “average viscous strain rate” during primar...](#)

[Figure 5.24 A comparison of experimental and calculated results for CS creep...](#)

[Figure 5.25 SRRT curves on a single specimen of IN-738LC at 1273 K for 161 M...](#)

[Figure 5.26 SRRT curve for IN-738LC \(a\) \$t_{rlx}\$ of 100 s under 497 MPa at 1123 ...](#)

[Figure 5.27 Dependence of des, \$\varepsilon_d\$ on \$\ln\(t_{rlx} + 1\)\$. \$\(\sigma/E\)s\$, for \$s = 4...\$](#)

[Figure 5.28 Stress dependence of viscous strain rate, \$\dot{\varepsilon}_v\$, during "primary cr...](#)

[Figure 5.29 Calculated stress-strain diagrams for Ti-6246 at 1005 K for a fe...](#)

[Figure 5.30 Predicted strain-rate dependence of 0.2% offset yield stress for...](#)

[Figure 5.31 Calculated total and three components of strain for constant str...](#)

[Figure 5.32 Calculated stress-strain diagrams for Waspaloy at 1005 K for a f...](#)

[Figure 5.33 Predicted strain-rate dependence of 0.2% offset yield stress for...](#)

[Figure 5.34 Calculated total and three components of strain for constant str...](#)

[Figure 5.35 Predicted strain-rate dependence of the total strain and the com...](#)

[Figure 5.36 Strain-rate dependence of ratio of \$\varepsilon_{d,Y}\$ and \$\varepsilon_{v,Y}\$ \(at ...](#)

[Figure 5.37 Schematic representations of shearing in precipitation-hardened,...](#)

[Figure 5.38 Cracks initiation at casting pores in CMSX-10. \(a\) Local stress ...](#)

[Figure 5.39 Four SRRT curves with recovery and two creep-fracture result for...](#)

[Figure 5.40 Corresponding data for the CMSX-10 SRRT curve at 1073 K, 700 MPa...](#)

[Figure 5.41 Delayed elastic strain recovery immediately after elastic recovery...](#)

[Figure 5.42 Long-term \(about 87 days\) des recovery after elastic recovery on...](#)

[Figure 5.43 Temperature dependence of strain components \(note the log scale\)...](#)

[Figure 5.44 CMSX-10 test at an initial stress of 700 MPa and 1223 K \(a\) stra...](#)

[Figure 5.45 Temperature dependence of tertiary stage strain rate versus true...](#)

[Figure 5.46 Calculated results for CMSX-10 for initial stress of 700 MPa at ...](#)

[Figure 5.47 Fractured specimens after creep-fracture tests on \[001\]-oriented...](#)

[Figure 5.48 Strain-time curves for five creep-fracture tests on \[001\]-orient...](#)

[Figure 5.49 Creep-fracture tests on \[001\]-oriented CMSX-10 single crystal at...](#)

[Figure 5.50 True stress versus mcr \(solid circles\) and tertiary strain rate ...](#)

[Figure 5.51 Calculated results for creep-fracture tests of CMSX-10 at 1173 K...](#)

[Figure 5.52 Plots of \$\dot{\epsilon}/\dot{\epsilon}_{0.01}\$ \(for 500, 550, and 600 MPa\), \$\dot{\epsilon}/\dot{\epsilon}_{0.015}\$ \(for 660 MPa\), and \$\dot{\epsilon}/\dot{\epsilon}_{0.105}\$ \(f...](#)

[Figure 5.53 Strain rate versus actual stress for CMSX-10 at 1123 K for 580 M...](#)

[Figure 5.54 Dependence of total engineering strain at fracture and fracture ...](#)

[Figure 5.55 CMSX-10 specimen tested at 1173 K and 700 MPa \(a\) diameter across...](#)

[Figure 5.56 Eccentricity of the cross-section along the length of the five f...](#)

[Figure 5.57 Distribution of cross-sectional area for the five creep ruptured...](#)

[Figure 5.58 Stress distribution along the gauge length at the time of fractu...](#)

[Figure 5.59 Dependence of local and estimated average stress at fracture on ...](#)

[Figure 5.60 Influence of orientation on the constant load stress-rupture pro...](#)

[Figure 5.61 Strain rate as a function of true stress up to fracture for <001...](#)

[Figure 5.62 Strain rate versus actual stress for CMSX-4 for 1000 °C. \(a\) 200...](#)

[Figure 5.63 Strain rate versus actual stress from constant load creep data o...](#)

[Figure 5.64 True strain rate versus true stress for TMS 75 for 900 °C, data ...](#)

[Figure 5.65 Strain rate versus actual stress for single crystal SRR99 for 98...](#)

Chapter 6

[Figure 6.1 Primary \(preprimary stage is too small to notice here\), secondary...](#)

[Figure 6.2 Time dependence of strain rate and true stress for the constant-l...](#)

[Figure 6.3 Strain rate versus true stress for the constant-load creep curve ...](#)

[Figure 6.4 Spherical void in undeformed section \(a\), stretched void with cra...](#)

[Figure 6.5 Compression stress-strain diagrams for directionally solidified \(](#)

[Figure 6.6 Initially transparent specimens \(100 × 250 × 50 mm, weighing 1.25...](#)

[Figure 6.7 Stress and strain histories, exhibiting initial recovery of delay...](#)

Chapter 7

[Figure 7.1 SEMs of replicas produced by dual process of etching and replicat...](#)

[Figure 7.2 SEM of a replica illustrating dislocation pileups in grain A indu...](#)

[Figure 7.3 First visible crack, substantiated by a large AE event, initiated...](#)

[Figure 7.4 Thin section \(0.8 mm thick\) showing open grain-boundary cracks \(b...](#)

[Figure 7.5 Horizontal \(a\) and vertical \(b\) thin sections of DS transversely ...](#)

[Figure 7.6 Columnar-grained S-2 ice at 243 K \(0.89 \$T_m\$ \) for a constant crossh...](#)

[Figure 7.7 Stress-rate dependence of stress at first visible cracks, substan...](#)

[Figure 7.8 Visually observed first crack produced in DS, S-2 ice at 263 K un...](#)

[Figure 7.9 Formation of the first cracks in S-2 ice at 263 K. \(a\) Dependence...](#)

[Figure 7.10 Formation of the first cracks in S-2 ice at 242 K. \(a\) Dependenc...](#)

[Figure 7.11 Temperature dependence of the critical delayed-elastic strain fo...](#)

[Figure 7.12 Formation of the first cracks in ice at 263 K for grain diameter...](#)

[Figure 7.13 Predicted stress and temperature dependence of apparent activati...](#)

[Figure 7.14 Experimental and theoretical predictions of creep of S-2 ice at ...](#)

[Figure 7.15 Theoretical crack density versus strains at \$0.96 T_m\$ for chosen g...](#)

Chapter 8

[Figure 8.1 Schematic of cracks in solids under compressive stress. \(a\) Penny...](#)

[Figure 8.2 Idealized cross-section of grain-facet-sized crack, with width \$w\$...](#)

[Figure 8.3 Theoretical stress, crack density, and strain including elastic, ...](#)

[Figure 8.4 Theoretical stress, crack density, and strain including elastic, ...](#)

[Figure 8.5 \(a\) EDEV-based theoretical outcomes.\(b\) Experimental observat...](#)

[Figure 8.6 Theoretical \(EDEV-based\) strain-rate dependence of crack density ...](#)

[Figure 8.7 EDEV-based strain-rate dependence of total strain and its elastic...](#)

[Figure 8.8 Theoretical, EDEV-based constant stress creep and creep rate curv...](#)

[Figure 8.9 Stress dependence of creep and crack density, \$N\$, predicted by EDE...](#)

[Figure 8.10 Strain rates and cracking activity at 0.96 \$T_m\$ for a stress of 2 ...](#)

[Figure 8.11 Computed crack-enhanced stress and time dependence of overall cr...](#)

[Figure 8.12 Theoretical time, stress, and grain size dependence of constant-...](#)

[Figure 8.13 Calculated grain size and time dependence of constant stress cre...](#)

[Figure 8.14 Grain size effect on constant load creep in stainless steel at 0...](#)

[Figure 8.15 EDEV-based theoretical strain and grain size dependence of \(a\) c...](#)

[Figure 8.16 Calculated dependencies of cracking activity. \(a\) Predicted grai...](#)

[Figure 8.17 Experimental creep in isotropic \(equiaxed\) ice with average grai...](#)

[Figure 8.18 Theoretical EDEV-based calculations for columnar-grained S-2 ice...](#)

[Figure 8.19 EDEV-based theoretical axial and volumetric strain for isotropic...](#)

[Figure 8.20 Calculated stress dependence of axial strain rate versus strain ...](#)

[Figure 8.21 Experimental stress dependence of axial and volumetric strain fo...](#)

[Figure 8.22 Experimental stress dependence of axial and volumetric strain un...](#)

[Figure 8.23 Deformation in directionally solidified \(DS\), columnar-grained m...](#)

[Figure 8.24 EDEV-based results for S-2 ice with a grain diameter of 1 mm at ...](#)

[Figure 8.25 EDEV-theory-based \(a\) stress-strain and volumetric strain-strain...](#)

[Figure 8.26 EDEV-based stress-strain diagram on repeat loadings for constant...](#)

[Figure 8.27 EDEV-based \(a\) strain, and \(b\) strain rate histories during five...](#)

[Figure 8.28 Calculated \(a\) microcracking, and \(b\) dilation histories for the...](#)

[Figure 8.29 A 3-D view of grain-boundary w-type cracks \(black\) and healed cr...](#)

Chapter 9

[Figure 9.1 Structure of IN-738LC. \(a\) Optical micrograph showing carbide pre...](#)

[Figure 9.2 Relaxation tests on Specimen-1 of cast, hot isostatically pressed...](#)

[Figure 9.3 Stress dependence of strain rate for IN-738LC at 1273 K from a si...](#)

[Figure 9.4 SEM of acicular or platelet microstructure of forged Ti-6246 used...](#)

[Figure 9.5 Interphase shearing processes. \(a\) \$\alpha\$ platelets \(A, B, C, and D\) c...](#)

[Figure 9.6 Experimental stress relaxation \(SR\) curves for Ti-6246 at 873 K o...](#)

[Figure 9.7 Strain-time \(left axis\) and stress-time \(right axis\) records duri...](#)

[Figure 9.8 Stress-strain diagram depicting loading and unloading for the SRT...](#)

[Figure 9.9 Ti-6246 at 873 K; each specimen was made from a new commercially ...](#)

[Figure 9.10 Experimental and theoretical dependence of \$n_{\text{SRT}}\$ of global strain...](#)

[Figure 9.11 Experimental and calculated results, including three strain comp...](#)

[Figure 9.12 Theoretical stress relaxation curves for Ti-6246 at 873 K corres...](#)

[Figure 9.13 Theoretical stress dependence of global strain rate for forged T...](#)

[Figure 9.14 Theoretical strain components for Ti-6246 at 873 K for SRT at co...](#)

[Figure 9.15 Theoretical dependence of “global rate/viscous rate” for strain ...](#)

[Figure 9.16 Theoretically predicted dependence of global rate/viscous rate o...](#)

[Figure 9.17 Theoretical and experimental results at unloading time of 600 s ...](#)

[Figure 9.18 Theoretical stress relaxation curves for pure polycrystalline ic...](#)

[Figure 9.19 \(a\) Theoretical stress relaxation curves of Figure 9.18 in terms...](#)

[Figure 9.20 Temperature dependence of stress relaxation in ice for a constan...](#)

[Figure 9.21 Theoretical stress relaxation curves at 263 K \(\$0.96 T_m\$ \) under a ...](#)

[Figure 9.22 Strain components \(elastic, delayed elastic, and viscous\) during...](#)

[Figure 9.23 Grain-size effect on the time dependence of \(a\) delayed elastic ...](#)

[Figure 9.24 Macrophotography of cross-sectional grain structure of DS, colum...](#)

[Figure 9.25 \(a\) Shearing of intergranular grain-boundary surfaces causing "m...](#)

Chapter 10

[Figure 10.1 Schematic depictions of the northern section of North America \(a...](#)

[Figure 10.2 Land emergence at two areas in Canada during the last 9000 years...](#)

[Figure 10.3 Dow's Lake ice cover deflection \(curve "a"\) and surface strain \(...\)](#)

[Figure 10.4 Dow's Lake ice swimming pool load test site illustrating four di...](#)

[Figure 10.5 Dow's Lake ice swimming pool load test load application history...](#)

[Figure 10.6 Dow's Lake ice swimming pool load test. \(a\) Deflection history r...](#)

[Figure 10.7 Surface strains measured at a distance of 4.5 m from the center ...](#)

[Figure 10.8 Dow's Lake ice swimming pool test carried out on 27 February 198...](#)

[Figure 10.9 Time dependence of deflection at 3, 6, 9, and 15 m from load cen...](#)

[Figure 10.10 Vertical deflection profiles along the survey line, obtained by...](#)

[Figure 10.11 Effect of grain size on calculations and comparison with measur...](#)

[Figure 10.12 Theoretical and experimental results for the Dow's Lake ice swi...](#)

[Figure 10.13 Comparison between measured deflection histories and theoretica...](#)

Chapter 11

[Figure 11.1 Earth's major thermohaline circulation system of cold water \(blu...](#)

[Figure 11.2 SLAR image of the Crozier Channel on 21 October, 1981, recorded ...](#)

[Figure 11.3 Airborne SAR images of \(a\) ribbed or wavy Ward Hunt Ice Shelf an...](#)

[Figure 11.4 Airborne SAR image of Eastern Arctic first-year sea-ice cover wi...](#)

[Figure 11.5 Sea-ice sheet moving against an iceberg in the Arctic, \(a\) creat...](#)

[Figure 11.6 Photographs of converging sea-ice sheets creating rift valley an...](#)

[Figure 11.7 Photographs of fragmented young \(<0.3 m thick\) sea-ice sheet pro...](#)

[Figure 11.8 Volcanic eruption from measurements of oxygen isotope, melt perc...](#)

[Figure 11.9 Sketch of the temperature profile in a floating ice cover.](#)

[Figure 11.10 An assumed vertical temperature profile of Earth and melting po...](#)

[Figure 11.11 Vertical temperature profile of earth in homologous scale assum...](#)

[Figure 11.12 Time-temperature shift for event duration of 1 s at reference t...](#)

[Figure 11.13 K-W, India earthquake zone since 1962.](#)

[Figure 11.14 K-W area's major earthquake zone since 1962; \$D\$ and \$d\$ are effect...](#)

[Figure 11.15 "Hobson's Choice" ice island \(marked as No. 1 in Figure 11.3b\) ...](#)

[Figure 11.16 Medium-scale indenter and NRCC borehole indenter \(BHI\) in trenc...](#)

[Figure 11.17 \(a\) 21 s mini-scale test on MY sea ice at \$0.93 T_m\$ -pressure and ...](#)

[Figure 11.18 Crack-surface profile on the vertical and horizontal surfaces f...](#)

[Figure 11.19 Pressure and displacement history for medium-scale indentation ...](#)

[Figure 11.20 Crack-surface profile on the vertical plane for the medium-scal...](#)

topologically close-packed (TCP) precipitates [39](#), [51](#)
traditional stress relaxation tests [304](#)-306
transforming boundaries, tectonic plates [372](#)
transgranular cracks [4](#)
transient creep [266](#)-267, [305](#)
see also [primary creep](#)
transmission electron microscopy (TEM) [62](#)
triaxial compression tests [103](#)-104

trinities

- of civilization [2-3](#)
- classifications [30](#)
- of cracks [4](#)
- of creep [14-16](#)
- cryosphere [7-8](#)
- crystal structures [31-33](#)
- earth's structure [7](#)
- of fire [2-6](#)
- of fracture [238-239](#)
- glass structures [33-34](#)
- high-temperature deformation mechanisms [55-56](#)
- iron phases [49](#)
- material properties [29-30](#)
- precipitate classifications [39](#)
- rocks [44-45](#)
- states [30-31](#)
- of strain [14](#)
- tectonic plates [371-372](#)
- turbine blades [4, 6](#)
 - design loads [113](#)
 - repairability [52](#)
 - tertiary creep [15](#)
- twin boundary defects [39](#)

u

ultimate tensile strength (UTS) [218](#)
ultra-high-temperature ceramic-matrix composites [48](#)
uniaxial compression tests [103](#)
uniaxial creep, constitutive equations [318](#)-321
unidirectional freezing *see* [directional solidification](#)
upper yield, constant stress creep tests [291](#)-293
UTS *see* [ultimate tensile strength](#)

v

vacancies [37](#)
vertical temperature profiles, Earth/ice sheets [378](#)-381
viscous deformation [13](#), [14](#)-16
volcanoes [376](#)-378
volume defects [40](#)
volume diffusion [133](#)

w

w-type void healing [295](#)-298
Warna dam, reservoir-triggered seismicity [386](#)-391
Waspaloy
 material parameters [162](#)
 strain relaxation and recovery tests [162](#)-169, [178](#)-185
 yield strength at 1005 K [178](#)-185
water, phase diagram [46](#)

weldability, nickel-base superalloys [52](#)-53

y

yield strength

definition [218](#)

and high temperatures [95](#)

Ti-6246 at 873 K [178](#)

Waspaloy at 1005 K [178](#)-185

Young's modulus

determination [97](#)

frequency dependence [93](#)-95

glass [43](#)-44

z

Zachariasen's model [41](#)

Zener pinning [40](#)